

Received June 30, 2019, accepted July 15, 2019, date of publication July 18, 2019, date of current version August 6, 2019.

Digital Object Identifier 10.1109/ACCESS.2019.2929659

Active Contour Driven by Weighted Hybrid Signed Pressure Force for Image Segmentation

JIANGXIONG FANG^{1,2}, HUAXIANG LIU¹, LITING ZHANG¹, JUN LIU², AND HESHENG LIU¹

¹Jiangxi Province Key Laboratory for Digital Land, East China University of Technology, Nanchang 330013, China

²School of Geophysics and Measure Control Technology, East China University of Technology, Nanchang 330013, China

Corresponding authors: Jiangxiong Fang (fangchj2002@163.com) and Hesheng Liu (hsliu@vip.163.com)

The work was supported in part by the National Natural Science Foundation of China under Grant 61463005, Grant 61866001, Grant 21664002, and Grant 61463017, in part by the China Postdoctoral Science Foundation under Grant 2017M612163, in part by the Natural Science Foundation of Jiangxi Province under Grant 20181BAB211017 and Grant 20171BAB202028, in part by the Jiangxi Provincial Key Laboratory of Digital Land under Grant DLLJ201804, and in part by the Science and technology project of Jiangxi Provincial Department of Education under Grant GJJ170450 and Grant GJJ160539.

ABSTRACT This study presents a novel active contour model (ACM) driven by weighted global and local region-based signed pressure force (SPF) to segment images in the presence of intensity inhomogeneity and noise. First, an adaptive weighted global region-based SPF (GRSPF) function as the driving centers is designed based on the global image information, which is based on the normalized global intensity to update the weights of the inner and outer regions of the curve during iterations. Second, by introducing the normalized absolute local intensity differences as the weighs of the inner and outer regions, an adaptive weighted local region-based SPF (LRSPF) function is similarly defined. Third, instead of setting a fixed force, a force propagation function is introduced to automatically balance the interior and exterior forces according to the image feature. Meanwhile, by combing the adaptive GWSPF and LWSPF functions, a weighted hybrid region-based SPF function is defined, which can improve the efficiency and accuracy of the proposed model. The experimental results on real images demonstrate that the proposed model is more robust than the popular region-based ACMs for segmenting images with intensity inhomogeneity and noise. The code is available at <https://github.com/fangchj2002/WHRSPF>.

INDEX TERMS Image segmentation, active contour, signed pressure force, intensity inhomogeneity.

I. INTRODUCTION

Image segmentation is an elementary task in the field of image processing and widely applied in image analysis, computer vision, medical imaging, etc. [1]. Its aim is to divide a given image into several object regions where each region is homogeneous with regard to a certain characteristic, i.e. intensity, color, texture [2]. A number of image segmentation algorithms [3] have been designed for different applications. Among these algorithms, active contour model (ACM) [4]–[6] is one of the most effective image segmentation algorithms. Its advantage is that the model can deal with topological changes of contour curves. The evolving contour in the ACM is represented as the zero level set and driven towards object boundaries by minimizing the energy function.

The associate editor coordinating the review of this manuscript and approving it for publication was Senthil Kumar.

According to image feature used for the formulation of the energy function, the extensive ACMs can roughly be categorized into two classes: the edge-based ACMs [4], [5] and the region-based ACMs [7], [8]. The edge-based ACMs use image gradient to extract the object boundaries. Geodesic active contour (GAC) is one of the most popular edge-based ACMs. Its idea is to incorporate image gradient and geometrically active contour into curve evolution theory to construct an edge stopping function. As described in [9], they can extract the objects by gradient, but they are difficult to detect the objects from the images with noise and weak boundaries. Therefore, GAC is usually sensitive to weak edges and noise.

Unlike the edge-based ACMs, the region-based ACMs are constructed on the formulation of computing global image region information of the inner and outer regions of the evolving contour. Thus, they can obtain better segmentation performance for images in the presence of weak boundaries than the edge-based ACMs. As a special example, the C-V

model proposed by Chan and Vese [6] is one of the most popular region-based ACMs, which is based on Mumford-Shah (M-S) model [9]. The M-S model utilizes the global intensity difference between the average intensities of the inner and outer regions of the evolving curve to guide the contour moving toward the object boundaries. It can achieve the desired segmentation for homogeneous images. However, it is still a difficult task for the C-V model to effectively segment images with intensity inhomogeneity (abbreviated as InH).

To deal with intensity InH in given images, many improved methods based on the C-V model with local image information have been proposed. Li et al. [10], [11] put forward a local binary fitting (LBF) model driven by a local fitting energy with a Gaussian kernel function. Instead of computing all pixels in the entire image, the fitted pixel value for each pixel can be effectively calculated as the average intensity of its local neighboring pixels. But the LBF model needs to perform four convolution operations in each iteration, which greatly increases computational cost. Local statistical Mumford-Shah (LS-M-S) model proposed by Brox and Cremers [12] is introduced with the analytical expression of the smooth approximation via Gaussian convolution operation. The energy function is formulated via maximum a-posteriori (MAP) estimation of contours, then minimizing the energy function is carried out using the Euler-Lagrange equations of local region statistics. Followed by this idea, Zhang et al. [13] proposed a local image fitting (LIF) model based on Gaussian filtering function with a local fitted image. The LIF model maps the input image domain to another domain using the sliding window method. The local fitted image is used to approximate the input image, and the Gaussian convolution is used to regularize the level set function (LSF). Wang et al. [14] further proposed a novel fitted image called square fitted image (SFI) to approximate the local fitted image. The model takes advantage of two fitted images (SFI and LIF) to construct a local hybrid image fitting (LHIF) energy based on Kullback-Leibler divergence. Then, its energy functional is minimized by gradient descent. Later on, many global and local ACMs are proposed to approximate the real-world images with intensity InH, e. g. local likelihood image fitting (LLIF) energy model [15], local cosine fitting energy [16], local pre-fitting energy (LPE) [17], local C-V models [18]–[20] via Gaussian function. However, these models cannot obtain desired segmentation results for highly noisy and inhomogeneous images.

On the other hand, hybrid active contour models by combining the edge-based and region-based ACMs have been designed in the literature. A variational model [21] with a GAC term and an edge-based term is proposed. In the model, a closed surface in a higher dimensional is represented as a zero LSF, which is embedded into the energy function to balance the average intensities of the interior and exterior regions. Li et al. [22] developed a novel type of level set evolution called distance regularization level set evolution (DRLSE), whose energy function includes a distance

regularization term and a data term. The distance regularization term with potential function can smooth the LSF and avoid the zero level curve disappearing, which drives level set evolution toward forward-and-backward (FAB) diffusion. Zhang et al. [23] proposed a novel region-based ACM with Selective Binary and Gaussian Filtering Regularized Level Set (SBGFLS). The ACM with SBGFLS uses the global statistical information of the exterior and interior of the evolving curve to construct a region-based signed pressure (SPF) function. The model penalizes level set function to be binary, and then uses a Gaussian filter to regularize it. Base on the Zhang's model, Talu et al. [24] proposed an Online Region-based Active Contour Model (ORACM). In the ORACM model, the gradient of the level set function is replaced with a user-defined LSF, which can be continually updated during iterations. To smooth the LSF, this model used the opening and closing morphological operations to remove the discontinuous regions. A global and local weighted signed pressure force based active contour (GL-SPF-AC) model [25] is introduced. In the model, an adaptive weighted SPF with a global weighted SPF (GWSPF) and a local weighted SPF (LWSPF) is designed to adjust the effect degrees of the GWSPF and the LWSPF. Hanbay and Talu [26] developed a new level set formulation to improve the segmentation performance of the LSFs by introducing the eigenvalue information of Hessian matrix into the LSF. The above models assumes that the intensity in given image is homogeneous. The global and local ACMs (GL-ACMs) [28]–[30] utilize the global intensity information and the local spatial information to segment the images with intensity InH. In addition, a fixed force in the ACM with SBGFLS [23], [24] is unreasonably set since all the given images cannot have the same feature. Therefore, it is still difficult for these models to accurately extract the object regions from images with severe intensity InH and noise.

In light of above analysis, we propose a new active contour driven by Weighted Hybrid Region-based SPF to segment images in the present of intensity InH and noise, called WHSPF. Our main contributions are as follows:

(1) By introducing the normalized global intensity as the coefficients of the inner and outer region of the evolving curve, an adaptively weighted global region-based SPF (GRSPF) function as the driving centers is defined based on the global pixel information, which avoids the difficulty of the parameter settings and improves the ability of handling intensity InH.

(2) Similar to the formulation of the GRSPF function, by introducing the normalized absolute local intensity differences of the inner and outer local regions of the evolving curve, an adaptive weighted local region-based SPF (LRSPF) function is defined.

(3) By combining the weighted GRSPF and LRSPF, a weighted hybrid region-based SPF function is defined. Moreover, instead of using a fixed force, a force propagation function is introduced based on the global image information of the evolving curve, which can automatically change the force during iteration.

II. PREVIOUS WORKS

A. C-V MODEL

The C-V model [6] proposed by Chan and Vese is a piecewise constant model and based on the Mumford-Shah model [9]. Let $I(x) : \Omega \rightarrow R$ be a given gray level image with pixel x , and $C : [0, 1] \rightarrow \Omega$ be a close contour, which divides the image domain into two regions: the internal region C_{in} and the external region C_{out} . The energy functional is written as

$$E^{CV}(C, c_1, c_2) = \mu \cdot \text{len}(C) + \lambda_1 \int_{C_{in}} |I(x) - c_1|^2 dx + \lambda_2 \int_{C_{out}} |I(x) - c_2|^2 dx \quad (1)$$

where the constants c_1 and c_2 are average intensities of the internal region C_{in} and the external region C_{out} , respectively, λ_1, λ_2 and μ are three positive constants, and $\text{Len}(C)$ denotes the length penalty term.

To minimize the energy functional, the minimization problem of the energy functional can be converted to solving a level set evolution equation. The level set method is defined by the curve C as the zero level set of a Lipschitz function, $\phi(x)$, such that:

$$\begin{cases} \phi(x) > 0 & \text{if } x \in \text{Inside}(C) \\ \phi(x) = 0 & \text{if } x \in \text{On}(C) \\ \phi(x) < 0 & \text{if } x \in \text{Outside}(C) \end{cases} \quad (2)$$

With the LSF defined in Eq. (2), the energy functional in Eq. (1) can be rewritten as:

$$E_\varepsilon^{CV}(c_1, c_2, \phi) = \mu \cdot \int_{\Omega} \delta_\varepsilon(\phi) |\nabla \phi| dx + \lambda_1 \int_{\Omega} (I(x) - c_1)^2 H_\varepsilon(\phi) dx + \lambda_2 \int_{\Omega} (I(x) - c_2)^2 (1 - H_\varepsilon(\phi)) dx \quad (3)$$

where ε is a positive constant, H_ε denotes the Heaviside function, $\delta_\varepsilon(\cdot)$ denotes the Dirac delta function, and they are defined as:

$$H_\varepsilon(x) = \frac{1}{2} \left[1 + \frac{2}{\pi} \arctan \left(\frac{x}{\varepsilon} \right) \right], \quad \delta(x) = \frac{dH(x)}{dx} = \frac{1}{\pi} \cdot \frac{\varepsilon}{\varepsilon^2 + x^2} \varepsilon \rightarrow 0 \quad (4)$$

The Euler-Lagrange equations are applied to solve the minimization problem with respect to the LSF ϕ . The gradient descent flow can be obtained using the Dirac delta function $\delta(\phi)$ with artificial time t , and the level set formulation can be written as:

$$\frac{\partial \phi}{\partial t} = \delta(\phi) \left(\mu \text{div} \left(\frac{\nabla \phi}{|\nabla \phi|} \right) - \lambda_1 (I(x) - c_1)^2 + \lambda_2 (I(x) - c_2)^2 \right) \quad (5)$$

with c_1 and c_2 equal to

$$c_1 = \frac{\int_{\Omega} H(\phi) I(x) dx}{\int_{\Omega} H(\phi) dx}, \quad c_2 = \frac{\int_{\Omega} [1 - H(\phi)] I(x) dx}{\int_{\Omega} (1 - H(\phi)) dx} \quad (6)$$

The optimal constants c_1 and c_2 can be far different from the original image with intensity InH.

B. ACM WITH SBGFLS

Zhang et al. [23] proposed a region-based ACM driven by the signed pressure function to segment images, which has the features of both the GAC model and the C-V model. The model with SBGFLS uses the average intensities of the inner and outer regions of the evolving curve as the driving center, and computes the difference between the intensity value and the driving center to drive the evolving curve toward the object boundaries. Then, it uses a Gaussian kernel function to smooth the level set function in each iteration. The SPF function is defined as:

$$spf(I((x))) = \frac{I(x) - \frac{c_1+c_2}{2}}{\max(|I(x) - \frac{c_1+c_2}{2}|)} \quad (7)$$

where c_1 and c_2 are defined in (6), respectively.

In Zhang's model, the edge stopping function is replaced with the SPF function in the GAC model. The evolving equation is written as follows:

$$\frac{\partial \phi}{\partial t} = spf(I(x)) \left(\text{div} \left(\frac{\nabla \phi}{|\nabla \phi|} \right) + \alpha \right) |\nabla \phi| + \nabla spf(I(x)) \cdot \nabla \phi \quad (8)$$

where α is a parameter of the speed to control the LSF updating, and $|\nabla \phi|$ is the gradient of the LSF.

In the process of implementation, a Gaussian filter is used to smooth the LSF and the regularization term is omitted. So the evolution curve is written as:

$$\frac{\partial \phi}{\partial t} = spf(I(x)) \cdot \alpha |\nabla \phi| \quad (9)$$

From Zhang's model, we can observe that the SPF function mainly depends on the difference between the image intensity and the fitted intensity of the inner and outer regions of the evolution curve. The model assumes that the intensities of the inner and outer regions in given image are homogeneous. However, it is difficult to segment images with complex intensity information, e.g. noise, intensity InH.

III. PROPOSED MODEL

In Zhang's model [23], the global image information is calculated as the driving center and suitable to segment the homogeneous images. In fact, the foreground and background regions in the real-world images are usually inhomogeneous. Therefore, the fixed constants, such as the weights of the intensity features of the internal and external regions, the updating speed α , are unreasonable. To solve these problems, by introducing the weighted global region-based SPF function and the weighted local region-based SPF function, we proposed a novel active contour model driven by weighted hybrid region-based signed pressure force to effectively segment inhomogeneous and noisy images.

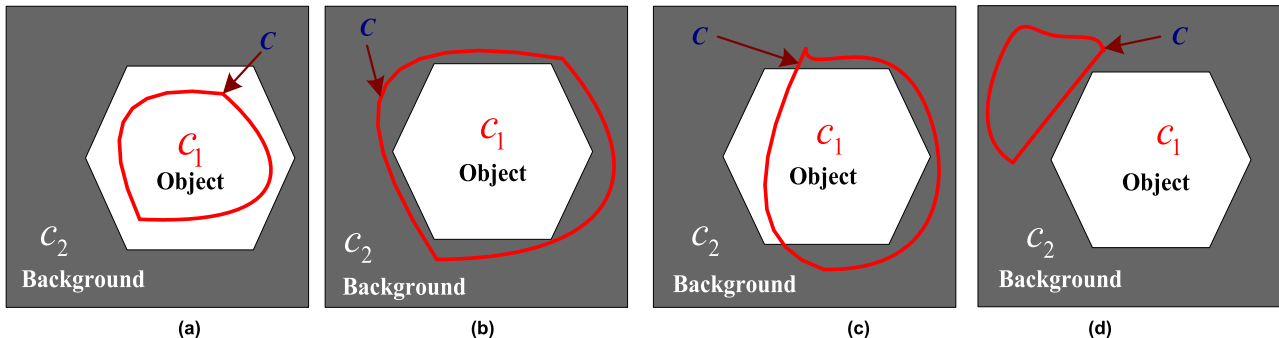


FIGURE 1. Different initial locations. (a) The evolving curve is completely inside the object region; (b)The evolving curve completely contains the object region; (c) The evolving curve intersects the object region; (d) The evolving curve is completely outside the object region.

A. WEIGHTED GLOBAL REGION-BASED SPF FUNCTION

In this section, we propose a novel formulation which is from the global image information. Different from the Zhang's model, by incorporating two average intensities of the inner and outer regions and the median intensity value of the inner region, we introduce a novel signed pressure force function based on the statistical pixel information to weight the inner and outer driving centers of the evolving curve. The global region-based signed pressure force (GRSPF) function is defined as:

$$\begin{aligned} & \text{spf}_{GR}(I(x)) \\ &= I(x) - \frac{w_{g1}(c_1+c_2)(c_1-c_2)+w_{g2}(m+c_2)(m-c_2)}{2(w_{g1}(c_1-c_2)+w_{g2}(m-c_2))} \\ &= I(x) - \frac{w_{g1}c_1^2+w_{g2}m^2-c_2^2}{2(w_{g1}c_1+w_{g2}m-c_2)} \quad (10) \end{aligned}$$

where w_{g1} and w_{g2} are two weighted constants and satisfies $w_{g1}+w_{g2}=1$, c_1 and c_2 are the average intensities inside and outside the regions of the evolving curve defined in Eq. (6), respectively, m is the median intensity value of the inner region. From Eq.(10), it is intuitive that the GRSPF function becomes the SPF function in the ACM with SBGFLS in [23] when the weight w_{g2} is set at 0, and it becomes the mean of the median intensity of the inner region and the average intensities of the outer regions when the weight w_{g1} is set at 0, which can reduce the influence of intensity InH. Three variables are defined as

$$\begin{cases} c_1 = \text{mean}(I(x) \in \{\mathbf{x} \in \Omega | \phi(\mathbf{x}) > 0\}) \\ c_2 = \text{mean}(I(x) \in \{\mathbf{x} \in \Omega | \phi(\mathbf{x}) < 0\}) \\ m = \text{median}(I(x) \in \{\mathbf{x} \in \Omega | \phi(\mathbf{x}) > 0\}) \end{cases} \quad (11)$$

where $I(x)$ is the input image of the pixel location x in the image domain Ω .

To adaptively update weighted parameters during iteration, two weighted constants are set according to the normalized global intensity, and defined as

$$w_{g1} = \frac{S_{in}}{S_{in} + S_{out}}, \quad w_{g2} = \frac{S_{out}}{S_{in} + S_{out}} \quad (12)$$

where S_{in} and S_{out} are the pixel number of the inner region and the outer region of the evolving curve.

The formulation of the GRSPF function in Eq. (10) is explained as follows. Assuming that the intensities of the object and background regions denotes c_o and c_b ($c_o > c_b$), and C denotes an arbitrary curve in given image. Four cases of the curve stopping positions are shown in Fig. 1. In Fig. 1(a), the evolving curve C is completely in the object region, the average intensity of the outer region is larger than that of the background region, and the median intensity of the inner region is equal to that of the inner region, namely $m = c_o = c_1$ and $c_2 > c_b$. The function is rewritten as:

$$I^{GSPF} = \frac{w_{g1}c_1^2 + w_{g2}m^2 - c_2^2}{2(w_{g1}c_1 + w_{g2}m - c_2)} = \frac{c_1 + c_2}{2} \quad (13)$$

It is intuitive that $c_2 < (c_o + c_b)/2 < I^{GSPF} = (c_1 + c_2)/2 < c_1$, which drives the evolving curve to expand toward the background region. On the contrary, in Fig. 1(b), the evolving curve contains the object region, the average intensity of the inner region is smaller than that of the object region ($c_o > c_1$), and the median intensity of the inner region is no less than that of the outer region ($m \geq c_2$). Therefore, we have $c_2 < I^{GSPF} < (c_o + c_b)/2 < c_1$. Intuitively, the force I^{GSPF} drives the evolving curve to shrink toward the object region. In Fig. 1(c), the situation is similar to Fig. 1(b), so we don't talk about it. In Fig. 1(d), the evolving curve is completely in the background region, the average intensity of the inner region is smaller than that of the object region, and the median intensity of the inner region is equal to that of the background region, namely $c_o > c_1$ and $m = c_b$. It is obvious that $c_2 < I^{GSPF} = (c_1 + c_2)/2 < (c_o + c_b)/2 < c_1$, which can drive the evolving curve to move toward the object boundaries.

B. WEIGHTED LOCAL REGION-BASED SPF FUNCTION

Similar to the formulation of the GRSPF function, to deal with image intensity InH, we introduce a weighted local region-based signed pressure force (LRSPF) function by incorporating pixel intensities of the inner and outer regions in local region. The LRSPF function is defined as

$$\text{spf}_{LR}(I(x)) = I(x) - (w_{l1}f_1 + w_{l2}f_2) \quad (14)$$

where w_{l1} and w_{l2} are two normalized absolute local intensity differences of the inner and outer regions, respectively.

Two variables w_{l1} and w_{l2} are defined as follows:

$$w_{l1} = \frac{d_{in}}{d_{in} + d_{out}}, \quad w_{l2} = \frac{d_{out}}{d_{in} + d_{out}} \quad (15)$$

where d_{in} and d_{out} are the number of the local absolute differences inside and outside the evolving curve in local region, and computed as:

$$\begin{cases} d_{in} = \text{Num}((I(x) - f_1) > 0) \\ d_{out} = \text{Num}((I(x) - f_2) < 0) \end{cases} \quad (16)$$

where f_1 and f_2 are two average intensities of the inner and outer local regions, which is defined as:

$$\begin{cases} f_1 = \text{mean}(I(y)|y \in \{W_k(x)(x \in \Omega_x) \cap \phi(y) > 0\}) \\ f_2 = \text{mean}(I(y)|y \in \{W_k(x)(x \in \Omega_x) \cap \phi(y) < 0\}) \end{cases} \quad (17)$$

where $y \in \Omega_x$ is a spatial point and independent of the center point x , Ω_x is a small neighborhood region centered at location x with a $(k+1) \times (k+1)$ square window, k is a positive integer. Here, $W_k(x)$ is represented as a Gaussian function with standard deviation σ and radius k .

As the same to formulation of the GRSPF function, the evolving curve moves toward the object boundaries, which can weight the local inner and outer driving centers and make segmentation performance more accurate.

C. LEVEL SET FORMULATION AND ITS ADVANTAGES

By combining the GRSPF function in Eq. (10) and the GLSPF function in Eq. (14), the hybrid region-based SPF function (HRSPF) is defined as:

$$spf_{HR}(I(x)) = w_g \cdot spf_{GR}(I(x)) + w_l \cdot spf_{LR}(I(x)) \quad (18)$$

where w_g and w_l are two weighted variables, which is used to balance the effects of the GRSPF and GLSPF functions. To make the same maximum of the GRSPF and GLSPF functions, the HRSPF function is rewritten as:

$$\begin{aligned} & spf_{HR}(I(x)) \\ &= w_g \cdot \min \left(1, \frac{\max(|spf_{GR}(I(x))|)}{maxspf} \right) \cdot spf_{GR}(I(x)) \\ &+ w_l \cdot \min \left(1, \frac{\max(|spf_{LR}(I(x))|)}{maxspf} \right) \cdot spf_{LR}(I(x)) \end{aligned} \quad (19)$$

where $maxspf = \max(|spf_{GR}(I(x))|, |spf_{LR}(I(x))|)$ is the maximum absolute value of the GRSPF and the LRSPF functions.

Unlike the ACM with SBGFLS [23] with a fixed force α , we use an adaptive force propagation function to control the force of the inner and outer regions of the curve. The force propagation function is defined as:

$$\alpha(I(x)) = |c_1 + m - 2c_2| \quad (20)$$

It is intuitive that the force propagation function can automatically balance the interior and exterior forces of the curve. More precisely, the propagation force increases when the evolving curve is far from the boundaries while the force decreases when the curve is close to the boundaries.

Following the SPF formulation in [23], the final level set formulation of our model is:

$$\begin{aligned} & \frac{\partial \phi}{\partial t} \\ &= spf_{HR}(I(x)) \cdot \alpha \cdot |\nabla \phi| = |c_1 + m - 2c_2| \\ &\cdot |\nabla \phi| \cdot \left(w_g \cdot \min \left(1, \frac{\max(|spf_{GR}(I(x))|)}{maxspf} \right) \cdot spf_{GR}(I(x)) \right. \\ &\left. + w_l \cdot \min \left(1, \frac{\max(|spf_{LR}(I(x))|)}{maxspf} \right) \cdot spf_{LR}(I(x)) \right) \end{aligned} \quad (21)$$

The proposed HRSPF model has the ability to modulate the sign of the pressure forces and implicitly control the propagation of the evolving curve. Or rather, the contour shrinks when it is outside the object of region of interest (ROI) while it expands when it is inside the object of ROI.

Compared with the popular ACMs, our proposed model has the following advantages:

1) Unlike the Zhang's model in Eq. (9), we introduce a force propagation function, which can be automatically tuned during iterations. When the evolving curve approaches the object boundaries during iterations, the value of the force propagation function automatically decreases.

2) Unlike the popular region-based ACM based on the C-V model with nonconvex energy function, the segmentation results are independent of initial curve. The HRSPF function is defined based on the global and local region-based intensity information, which causes the model independent of initial curve.

3) Two strategies are used to improve the robustness to intensity InH and noise. On the other hand, the median value of the inner region of the curve is closer to the pixel value of object boundaries when the images contains severe intensity inhomogeneity and noise. Therefore, one strategy is that the median value of the inner region is used to define the GRSPF function. The other strategy is that a local intensity information of images is used to reduce the effects of intensity InH and noise.

D. DESCRIPTION OF ALGORITHM STEPS

To illustrate the procedure of implementation, the main steps of our model is summarized as:

1. Specify a given image, and initial parameters: weighted constants w_g, w_l , the maximum number of iterations $IterNum$, the radius k and standard deviation σ of the local window in Eq. (17).

2. Initialize the level set function

$$\phi(x, t=0) = \begin{cases} \rho & x \in \Omega_b \\ -\rho & x \in \Omega - \Omega_b \end{cases} \quad (22)$$

where ρ is a positive constant, Ω_b is a subset of the image domain Ω .

3. Compute the variables of the GRSPF function: the average intensities of the inner and outer regions using Eq. (6), the median intensity value of the inner region m using Eq. (11), and two adaptive weighted parameters w_{g1} and w_{g2} using Eq. (12).

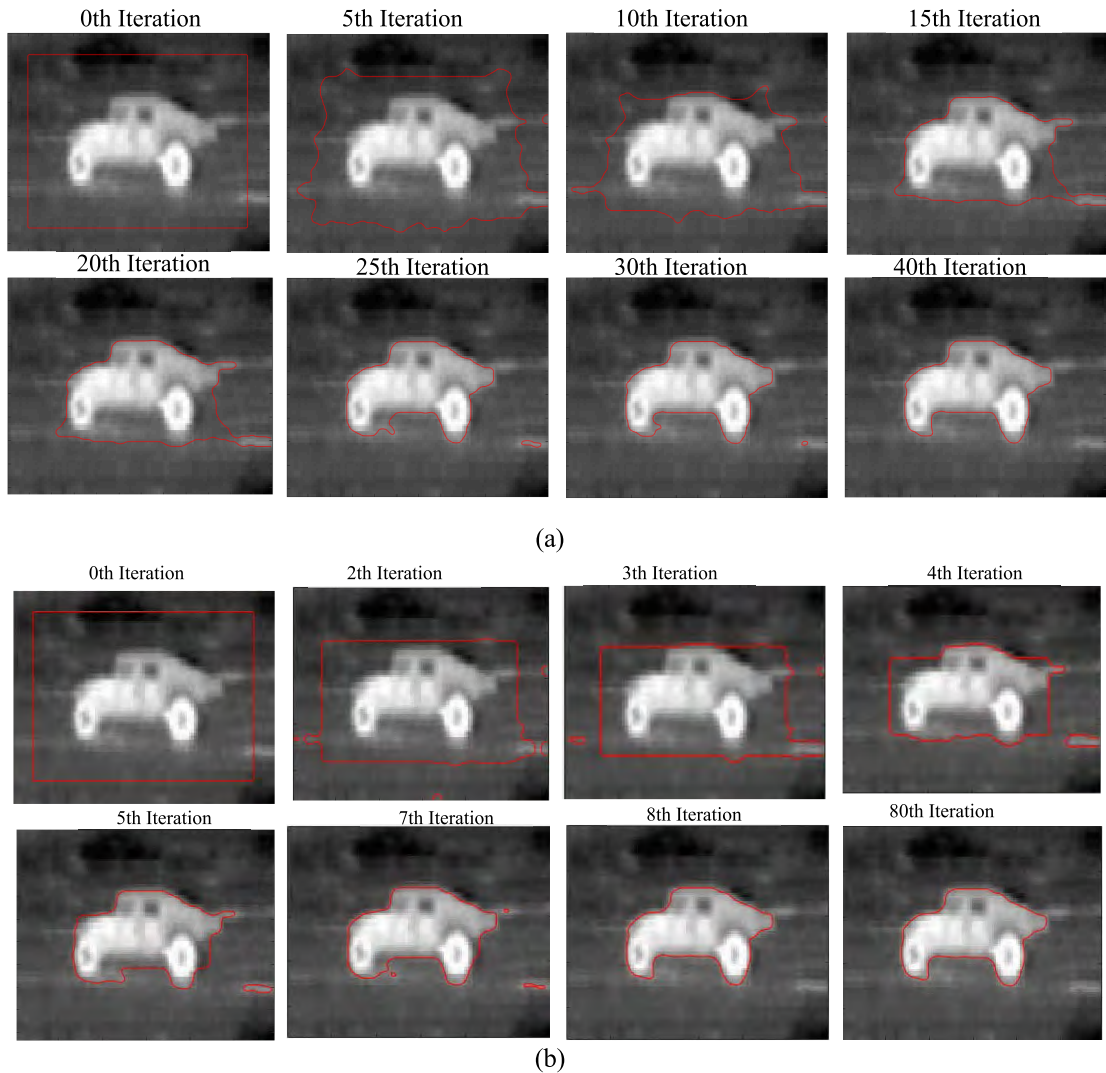


FIGURE 2. Segmentation results of (a) the ACM with SBGFRRLS ($\alpha = 25$) and (b) the proposed model.

4. Compute the variables of the LRSPF function: two average intensities of the local inner and outer regions f_1 and f_2 using Eq. (17), and two adaptive weighted parameters w_{l1} and w_{l2} using Eq. (14).

5. Compute the HRSPF function using Eq. (19) by combining the GRSPF and LRSPF functions using Eqs. (10) and Eq. (14).

6. Update the level set function in Eq. (21) by combining the force propagation function in Eq. (20).

7. Regularize and smooth the pseudo LSF using the Gaussian filter.

8. Repeat steps 3-7 till the iterations are finished.

IV. EXPERIMENTS AND RESULTS

In this section, we validate the performance of the proposed model on images in the presence of intensity InH and noise. To demonstrate the effectiveness of the proposed model, we compare the proposed model with the

popular ACMs, such as the C-V model [6], the ACM with SBGFRRLS [23], the LBF model [11], the LIF model [13], the ORACM [24] without and with morphological operations, the ACM with Hessian matrix (ACM-HM) [25], the global and local weighted SPF (GLW-SPF) [26]. The codes of the C-V and ORACM models can be downloaded from the url: <https://ww2.mathworks.cn/matlabcentral/fileexchange/49034-oracm-online-region-ased-active-contour-model>. The code of the ACM with SBGFRRLS and the LIF model can be download from the url: <http://www.kaihuazhang.net/>. The code of the proposed model is available at the website: <https://github.com/fangchj2002/WHRSPF>.

All of the ACM-based models are processed using a 3.2-GHz Intel 4-core PC computer with 3 GB of memory using the Matlab programming language. If no otherwise specif, the parameters in the proposed model are fixed as follows: the weighted constants $w_g = w_l = 0.5$, the Gaussian function with standard deviation $\sigma = 1.5$ and radius $k = 5$, and the maximal iteration number $IterNum = 40$.

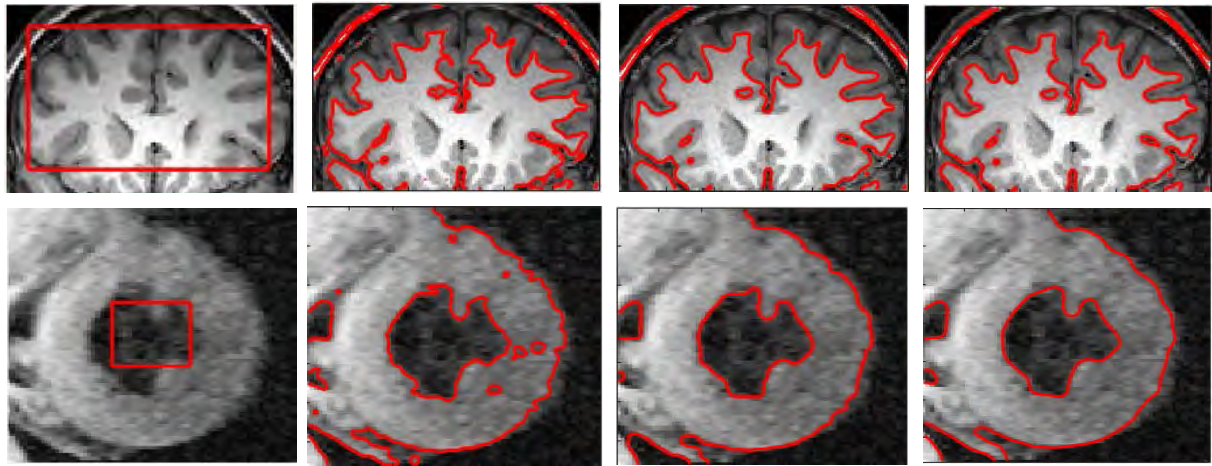


FIGURE 3. Segmentation results using the GRSPF model, the LRSFP model, and the HRSPF model, respectively. The 1st column: Initial contours with different shapes; From the 2nd column to 4th column: the final stopping positions corresponding to the GRSPF model, the LRSFP model, and the proposed model, respectively.

A. SEGMENTATION RESULTS ON REAL IMAGES

The first experiment is used to validate the efficiency of the proposed model compared with the ACM with SBGFLS. The ACM with SBGFLS with the force $\alpha = 25$ segments the image into two regions, and the segmentation results are shown in Fig. 2(a). It is intuitive that the evolving curves stops the object boundaries after 40 iteration. Fig. 2(b) shows the segmentation results of the HRSPF model for the same image with the same initial curve. We can find that the evolving curve in our HRSPF model arrives at the object boundaries after only eight iterations. By using the level set formulation in Eq. (19) with the force propagation function, our model converges faster than the ACM with SBGFLS.

The following experiments will examine the effects of the weighted GRSPF model and the LRSFP model, respectively. The level set formulation of the GRSPF and LRSFP models are written as:

$$\begin{aligned} \text{GRSPFmodel : } & \frac{\partial \phi}{\partial t} \\ &= spf_{GR}(I(x)) \cdot \alpha(I(x)) \cdot |\nabla \phi| \\ &= |c_1 + m - 2c_2| \cdot |\nabla \phi| \cdot \left(I(x) - \frac{w_{g1}c_1^2 + w_{g2}m^2 - c_2^2}{2(w_{g1}c_1 + w_{g2}m - c_2)} \right) \\ \text{LRSFPmodel : } & \frac{\partial \phi}{\partial t} \\ &= spf_{LR}(I(x)) \cdot \alpha(I(x)) \cdot |\nabla \phi| \\ &= |c_1 + m - 2c_2| \cdot |\nabla \phi| \cdot (I(x) - (w_{l1}f_1 + w_{l2}f_2)) \end{aligned} \quad (23)$$

Fig. 3 demonstrates the segmentation results on two medical images using the GRSPF model, the LRSFP model and the HRSPF model, respectively. Three models with the same initial curves are shown in the 1st column. From the 2nd column to 4th column, the final stopping positions of the evolving curves corresponds to the GRSPF model, the LRSFP model, and the HRSPF model, respectively. As can be seen in Fig. 3, it is obvious that the GRSPF model can extract more detailed information than the LRSFP model. More precisely,

the GRSPF model can extract more detailed object regions while the LRSFP model detects some large regions. By incorporating the GRSPF and the LRSFP model, the proposed model can accurately detect object boundaries.

B. ROBUSTNESS TO NOISY IMAGES

The aim of the experiment was to testify the robustness of the proposed model to segment images in the presence of noise. We compare the proposed model with the popular ACMs on different level noisy images including Gaussian noise, salt and pepper noise and speckle. Generally speaking, the real-world images are made up of the clean images corrupted by one or more types of the above noise. Fig. 4 shows the segmentation results with three different types of noise. In the 1st row of Fig. 4, four images denotes the clean image, the clean image corrupted by Gaussian noise with zero mean and the variances of 0.05, pepper noise with densities of 0.03, random speckle noise with zero mean and the variances of 0.05, respectively. Therefore, accurately extracting the desired objects from these images with severe noise is a challenging task. From the 2nd row to the 7th row, the final stopping boundaries are shown using the C-V model, the ACM with SBGFLS [23], the ORACM without morphological operations (ORACM NMO), the ORACM with morphological operations (ORACM WMO), the ACM-HM, and the proposed model, respectively. It is noted that only the proposed model can exactly extract all of the objects in four images. The C-V model has the worst results since its nonconvex energy function makes the segmentation results stuck in local minima. These models except for the C-V model can accurately detect the objects from the clean image. The ACM with SBGFLS fails to segment the noisy images since it assumes that the given image is homogeneous, and the ORACM without and with morphological operations cannot both accurately extract the objects from two noisy images. Remarkably, the ACM-HM can decrease the effect of the

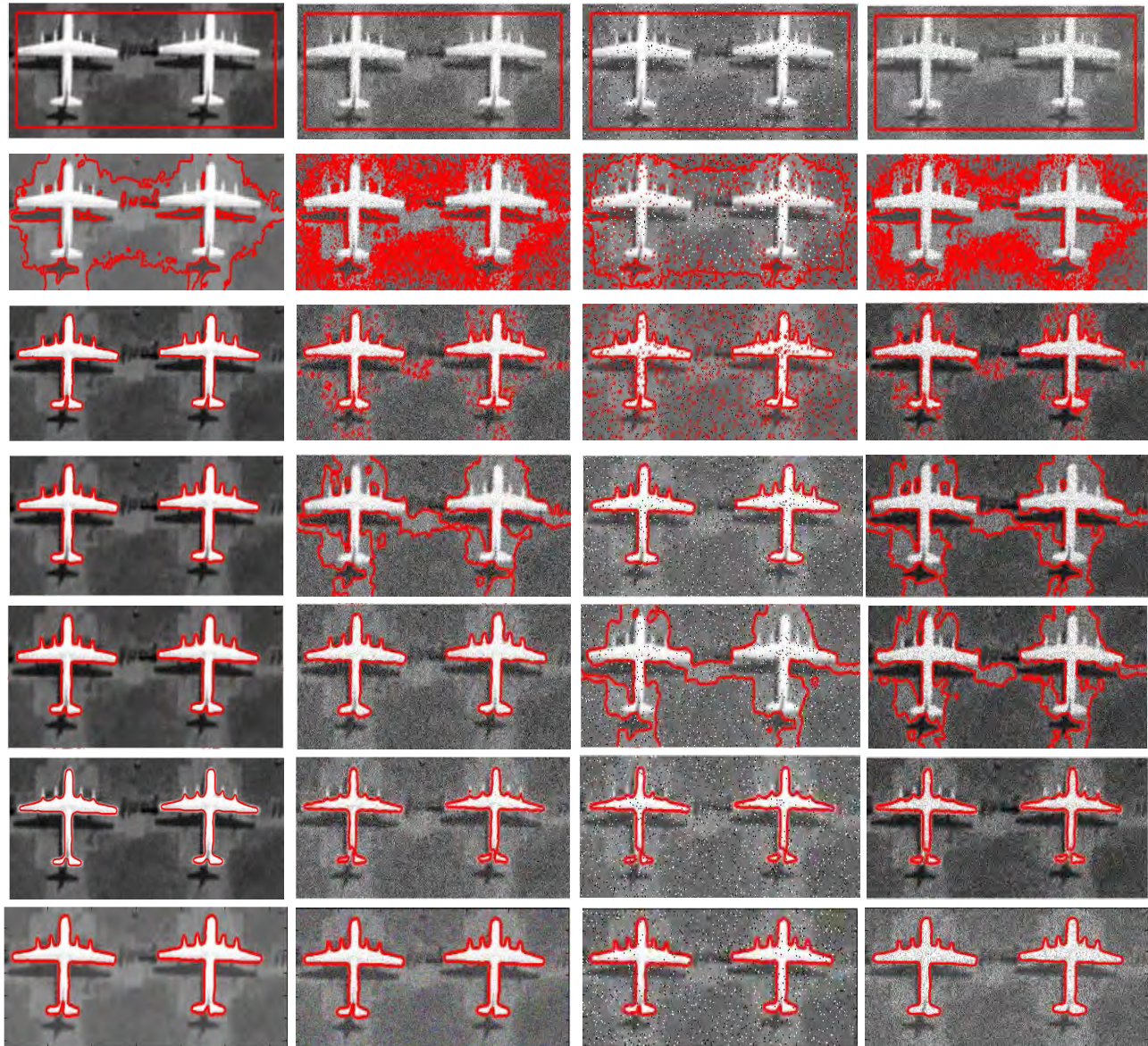


FIGURE 4. Segmentation results using different ACMs by adding different types of noise. In the 1st row: The input images with initial contours; From the 2nd row to the 7th row: The final stopping positions using the C-V model, ACM with SBGFRSL, the ORACM NMO model, the ORACM WMO model, and the proposed model.

noise while it can only extract the brightest regions due to its use of a second order derivative. In short, our model can achieve better segmentation performance for real images with different types of noise.

C. ROBUSTNESS TO INITIAL CURVES

The next experiment validates whether the segmentation results are sensitive to the initial curves or not. Fig.5 demonstrates the segmentation results on the same medical image with different initial shapes using the proposed model. In the 1st column, four initial curves with different positions are shown corresponding to a large rectangle, a small rectangle, a pentagon, and a triangle, respectively. From the 2nd column to the 4th column, the stopping positions of the curves

during 5, 10, and 15 iterations, respectively, are shown. The final stopping positions are shown in the 5th column. As can be seen from the results, the objects can be partitioned into similarly segmented regions with different initial curves. From the above results, it is obvious that the proposed algorithm can achieve desired segmentation. In a word, the proposed model is independent of initial curves.

D. COMPARISON WITH THE POPULAR ACMs

To quantitatively evaluate the ACMs, we use region entropy [27] to measure performance without ground truth. The region entropy is defined as:

$$RE = E_l(I) + E_r(I) \quad (24)$$

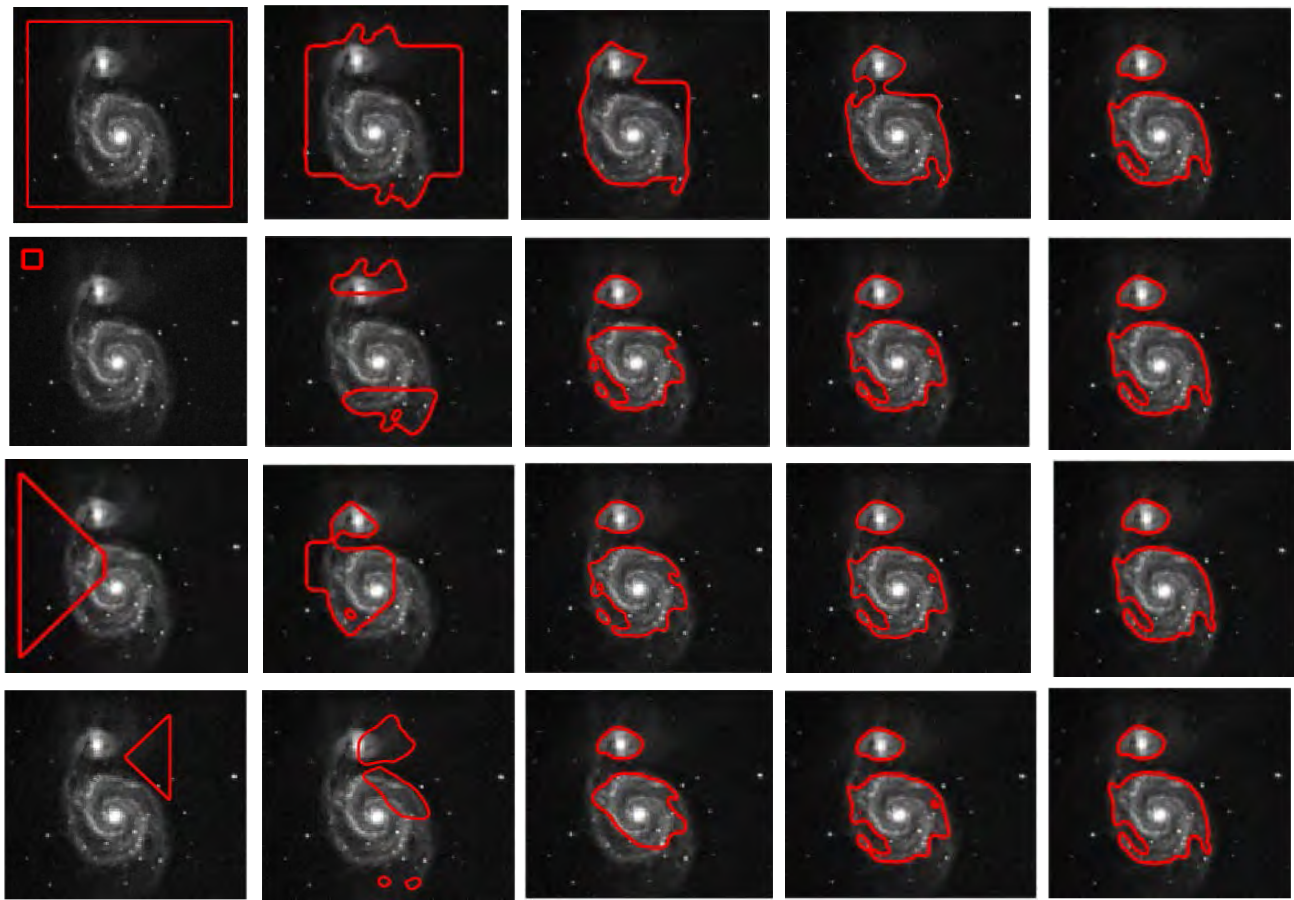


FIGURE 5. Segmentation results for medical image with different initial curves. In the 1st column: Initial contours with different shapes; From the 2nd column to 4th column: The stopping positions of the curves during 5, 10, and 15 iterations, respectively; The 5th column: The final stopping positions of the curves.

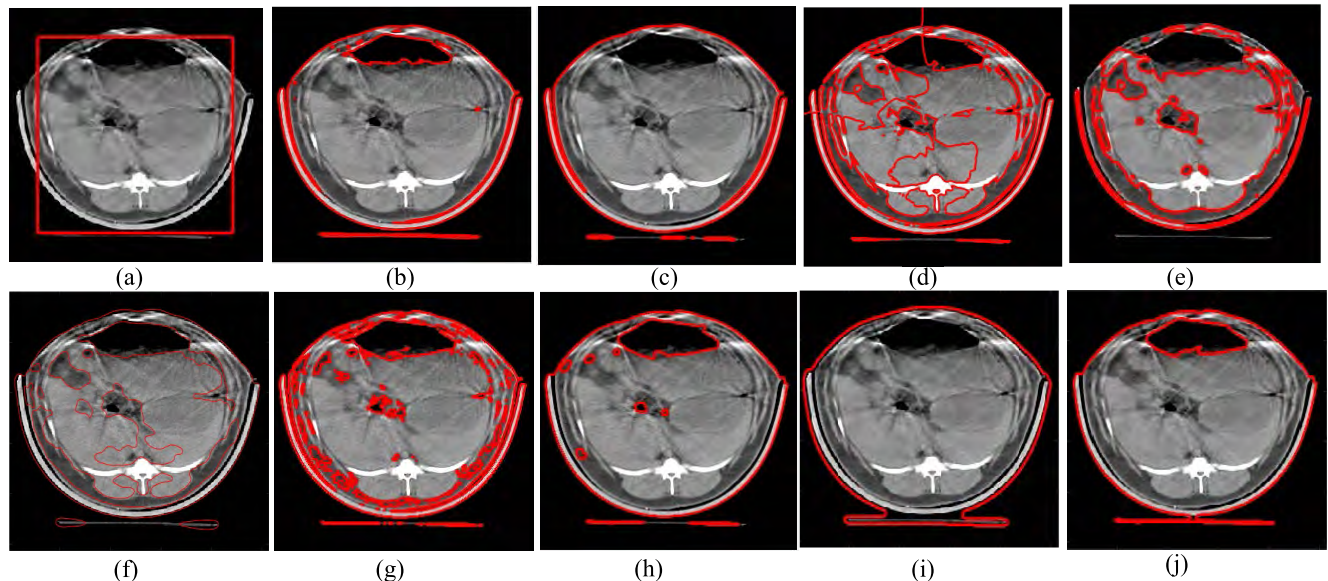


FIGURE 6. Segmentation results for medical image using different ACMs. (a) The Input image with initial curve; (b) C-V; (c) ACM with SBGFRLS; (d) LBF; (e) ACM-HM; (f) LIF; (g) ORACM-NMO; (h) ORACM-WMO; (i) GLW-SPF; (j) WHRSPF.

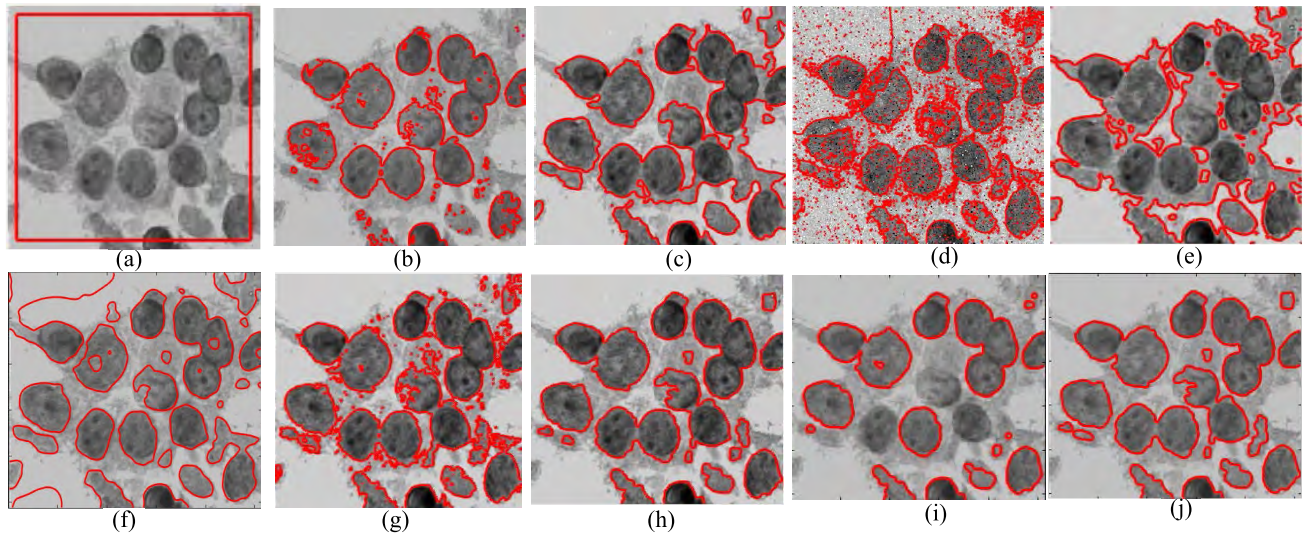


FIGURE 7. Segmentation results for medical image using different ACMs. (a) The Input image with initial curve; (b) C-V; (c) ACM with SBGFRLS; (d) LBF; (e) ACM-HM; (f) LIF; (g) ORACM-NMO; (h) ORACM-WMO; (i) GLW-SPF; (j) WHRSPF.

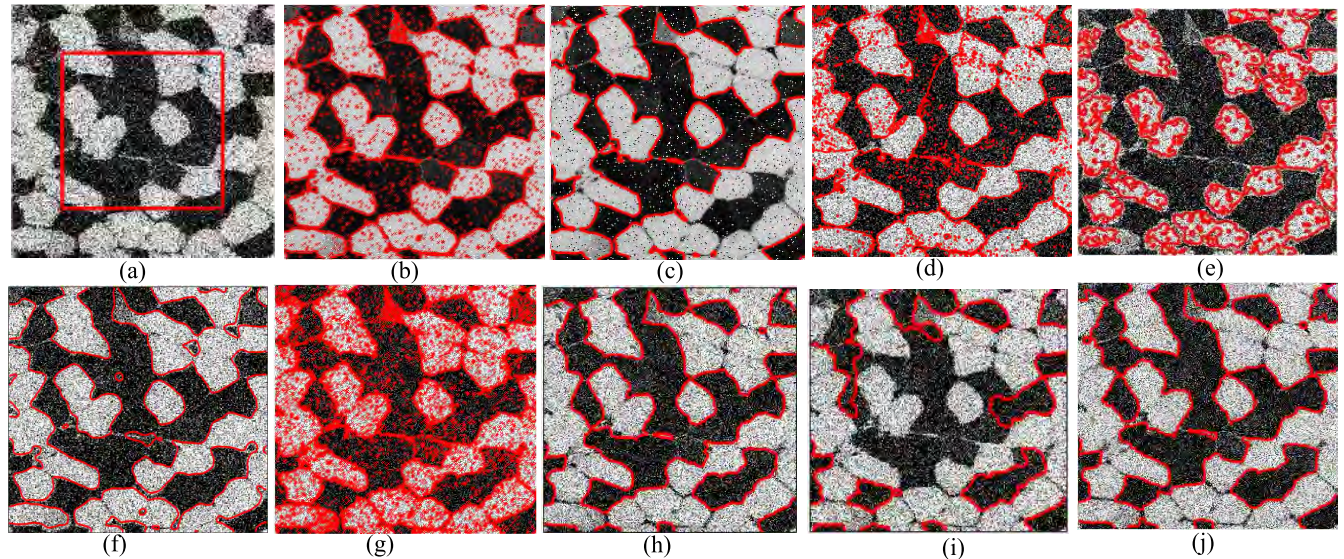


FIGURE 8. Segmentation results for medical image using different ACMs. (a) The Input image with initial curve; (b) C-V; (c) ACM with SBGFRLS; (d) LBF; (e) ACM-HM; (f) LIF; (g) ORACM-NMO; (h) ORACM-WMO; (i) GLW-SPF; (j) WHRSPF.

where $E_l(I)$ and $E_r(I)$ are a layout entropy and an desired region entropy, respectively.

Here, $E_l(I)$ and $E_r(I)$ are defined as follows:

$$E_l(I) = - \sum_{i=1}^N \left(\frac{S_i}{S_I} \right) \log \left(\frac{S_i}{S_I} \right) \quad (25)$$

$$E_r(I) = - \sum_{i=1}^N \left(\frac{S_i}{S_I} \right) \sum_k \left(\frac{L_i(k)}{S_i} \right) \log \left(\frac{L_i(k)}{S_i} \right) \quad (26)$$

where S_i/S_I is the probability of a pixel belong to region R_i , and $L_i(m)$ is the number of pixels in region R_i which has value k of a luminance.

To further validate the robustness of the proposed model, the following experiments is performed on the biomedical images from the biomedical database available at url:

<http://decsai.ugr.es/cvg/dbimagenes/gbio256.php>. Compared with the popular ACMs, the segmentation results of the proposed model on images with different intensity characteristics is shown in Figs. 6-7. To verify the robustness to noise, the images in Figs. 8-9 are corrupted by Gaussian noise with mean 0 and variance 0.05, and Gaussian noise with mean 0 and variance 0.005, followed by salt and pepper noise with a density of 0.05. Therefore, it is accurately a challenging task to extract the desired objects from the images with severe inhomogeneity and noise.

As can been seen from Figs. 6-9, the proposed model can accurately extract the objects from four biomedical images. To quantitatively present the segmentation performance, comparative results in terms of average running time and region entropy are shown in Tables 1-2. In terms of accuracy from these figures and Table. 1, it is intuitive that

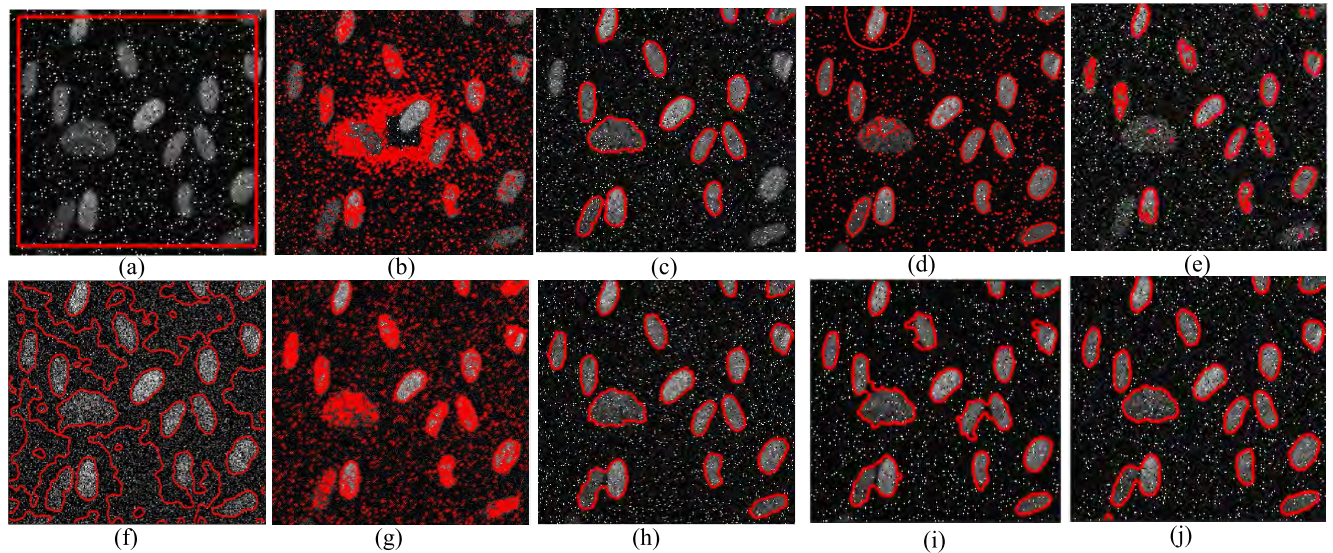


FIGURE 9. Segmentation results for medical image using different ACMs. (a) The Input image with initial curve; (b) C-V; (c) ACM with SBGFRRLS; (d) LBF; (e) ACM-HM; (f) LIF; (g) ORACM-NMO; (h) ORACM-WMO; (i) GLW-SPF; (j) WHRSPF.

TABLE 1. Comparison of the region-based ACMs in terms of region entropy.

Image	C-V	ACM with SBGFRRLS	LBF	ACM-HM	LIF	ORACM NMO	ORACM WMO	GLW-SPF	Our
Fig. 6	4.649	5.219	6.232	4.849	5.624	5.863	4.746	4.748	4.314
Fig. 7	4.872	5.028	6.434	4.986	5.785	5.794	4.421	4.827	4.378
Fig. 8	5.514	4.954	5.976	5.790	4.837	6.074	4.358	5.149	4.286
Fig. 9	6.146	5.428	6.087	5.548	5.926	5.871	4.387	4.527	4.209

TABLE 2. Comparison of the region-based ACMs in terms of running time(Seconds).

Image	Fig. 6		Fig. 7		Fig. 8		Fig. 9	
	Iteration	Time	Iteration	Time	Iteration	Time	Iteration	Time
C-V	19.877	207	29.783	251	42.092	196	67.722	320
ACM with SBGFRRLS	5.411	76	3.602	53	4.018	55	13.046	151
LBF	24.124	200	23.563	200	25.619	200	24.826	200
ACM-HM	6.340	50	6.750	50	9.164	50	7.363	50
LIF	37.416	200	37.099	200	38.118	200	38.119	200
ORACM NMO	1.926	10	1.565	16	1.193	10	1.374	10
ORACM WMO	0.574	8	1.032	14	0.614	10	0.778	10
GLW-SPF								
Our	2.048	40	3.018	40	1.327	40	1.531	40

the C-V model and the ORACM-NMO model have too many small regions since they assume that the object region is homogeneous and ignores the intensity differences of the local regions. In addition, the ACM with SBGFRRLS based on the global image information cannot extract the objects from complex noisy image. The ORACM-WMO model can obtain better results than the ORACM-NMO, LBF, LIF, ACM-HM, and GLW-SPF models because the morphological operations can reduce effects of noise during iteration. However, the ORACM-WMO model perhaps appears small regions where the pixel number is larger than the threshold. The ACM-HM integrates the eigenvalue information of Hessian matrix into the level set function, whose second order derivative is sensitive to noise and cannot accurately

extract the objects from the noisy images shown in Fig. 8(e) and Fig. 9(e). In terms of segmentation accuracy from Table. 1, only the proposed model can extract all the objects in Figs. 6-9.

E. COMPUTATIONAL COMPLEXITY

In the following, we discuss the computational complexity of the proposed model. Assuming the number of pixels in the segmented image is N , the size of the local window radius is k , which is usually negligible since $k \ll N$. From Eq. (23), it is intuitive that the complexity of the GRSPF model is $O(N)$. and the complexity of the LRSPF model in Eq. (23) $O(k^2N)$. The proposed model is constructed by incorporating the GRSPF model and the LRSPF model. Therefore,

the computational complexity of the proposed model $O((k^2 + 1)N) \approx O(N)$.

It is also seen that the C-V model, the LBF model, and the LIF model take the more running time than other models. And the propose model takes minimum executing time while our model takes the least average time since the fixed iterations are set.

V. CONCLUSION

This paper introduces a novel active contour model driven by weighted hybrid region-based SPF to segment images in the present of intensity inhomogeneity and noise. Different from the ACM with SBGFLRS, the weighted hybrid region-based SPF function consists of an adaptive GRSPF function and an adaptive LRSPF function, and a force propagation function based on the global image information is introduced. By incorporating the global and local image information, the proposed model can accurately detect the object region from images with intensity InH and noise. Experimental results on real images demonstrate that the superiorities of the proposed model in terms of average running time and segmentation accuracy compared with the C-V model, ACM with SBGFLRS, the LBF model, ACM-HM, the ORACM-NMO model, and the ORACM-WMO model.

It is noted that our model is only applied to two-phase image segmentation. In the future, we will extend it to multi-phase image segmentation. In addition, the proposed model cannot segment 3D images directly. Therefore, another extension of our work is study 3D image segmentation.

REFERENCES

- [1] M. Singh, M. C. Govil, and E. S. Pilli, "CHACT: Convex hull enabled active contour technique for salient object detection," *IEEE Access*, vol. 6, pp. 22441–22451, 2018.
- [2] E. Karami, M. S. Shehata, and A. Smith, "Adaptive polar active contour for segmentation and tracking in ultrasound videos," *IEEE Trans. Circuits Syst. Video Technol.*, vol. 29, no. 4, pp. 1209–1222, Apr. 2019.
- [3] S. Niu, Q. Chen, L. de Sisternes, Z. Ji, Z. Zhou, and D. L. Rubin, "Robust noise region-based active contour model via local similarity factor for image segmentation," *Pattern Recognit.*, vol. 61, pp. 104–119, Jan. 2017.
- [4] M. Kass, A. Witkin, and D. Terzopoulos, "Snakes: Active contour models," *Int. J. Comput. Vis.*, vol. 1, no. 4, pp. 321–331, 1988.
- [5] V. Caselles, R. Kimmel, and G. Sapiro, "Geodesic active contours," *Int. J. Comput. Vis.*, vol. 22, no. 1, pp. 61–79, 1997.
- [6] T. F. Chan and L. A. Vese, "Active contours without edges," *IEEE Trans. Image Process.*, vol. 10, no. 2, pp. 266–277, Feb. 2001.
- [7] S. C. Zhu and A. Yuille, "Region competition: Unifying snakes, region growing, and Bayes/MDL for multiband image segmentation," *IEEE Trans. Pattern Anal. Mach. Intell.*, vol. 18, no. 9, pp. 884–900, Sep. 1996.
- [8] L. A. Vese and T. F. Chan, "A multiphase level set framework for image segmentation using the Mumford and Shah model," *Int. J. Comput. Vis.*, vol. 50, no. 3, pp. 271–293, Dec. 2002.
- [9] D. Mumford and J. Shah, "Optimal approximations by piecewise smooth functions and associated variational problems," *Commun. Pure Appl. Math.*, vol. 42, pp. 577–685, Jul. 1989.
- [10] C. Li, C. Xu, C. Gui, and M. D. Fox, "Level set evolution without re-initialization: A new variational formulation," in *Proc. IEEE Comput. Soc. Conf. Comput. Vis. Pattern Recognit.*, Jun. 2005, pp. 430–436.
- [11] C. Li, C.-Y. Kao, J. C. Gore, and Z. Ding, "Minimization of region-scalable fitting energy for image segmentation," *IEEE Trans. Image Process.*, vol. 17, no. 10, pp. 1940–1949, Oct. 2008.
- [12] T. Brox and D. Cremers, "On local region models and a statistical interpretation of the piecewise smooth Mumford-Shah functional," *Int. J. Comput. Vis.*, vol. 84, pp. 184–193, Aug. 2009.
- [13] K. Zhang, H. Song, and L. Zhang, "Active contours driven by local image fitting energy," *Pattern Recognit.*, vol. 43, no. 4, pp. 1199–1206, Apr. 2010.
- [14] L. Wang, Y. Chang, H. Wang, Z. Wu, J. Pu, and X. Yang, "An active contour model based on local fitted images for image segmentation," *Inf. Sci.*, vol. 418–419, pp. 61–73, Dec. 2017.
- [15] Z. Ji, Y. Xia, Q. Sun, G. Cao, and Q. Chen, "Active contours driven by local likelihood image fitting energy for image segmentation," *Inf. Sci.*, vol. 301, pp. 285–304, Apr. 2015.
- [16] J. Q. Miao, T. Z. Huang, X. B. Zhou, Y. G. Wang, and J. Liu, "Image segmentation based on an active contour model of partial image restoration with local cosine fitting energy," *Inf. Sci.*, vol. 447, pp. 51–71, Jun. 2018.
- [17] K. Ding, L. Xiao, and G. Weng, "Active contours driven by local pre-fitting energy for fast image segmentation," *Pattern Recognit. Lett.*, vol. 104, no. 1, pp. 29–36, Mar. 2018.
- [18] C. He, Y. Wang, and Q. Chen, "Active contours driven by weighted region-scalable fitting energy based on local entropy," *Signal Process.*, vol. 92, no. 2, pp. 587–600, Feb. 2012.
- [19] H. J. Wang and M. Liu, "Active contours driven by local Gaussian distribution fitting energy based on local entropy," *Int. J. Pattern Recognit. Artif. Intell.*, vol. 27, no. 6, 2013, Art. no. 1355008.
- [20] H. Ali, N. Badshah, K. Chen, and G. A. Khan, "A variational model with hybrid images data fitting energies for segmentation of images with intensity inhomogeneity," *Pattern Recognit.*, vol. 51, pp. 27–42, Mar. 2016.
- [21] M. Holtzman-Gazit, R. Kimmel, N. Peled, and D. Goldsher, "Segmentation of thin structures in volumetric medical images," *IEEE Trans. Image Process.*, vol. 15, no. 2, pp. 354–363, Feb. 2006.
- [22] C. Li, C. Xu, C. Gui, and M. D. Fox, "Distance regularized level set evolution and its application to image segmentation," *IEEE Trans. Image Process.*, vol. 19, no. 12, pp. 3243–3254, Dec. 2010.
- [23] K. Zhang, L. Zhang, H. Song, and W. Zhou, "Active contours with selective local or global segmentation: A new formulation and level set method," *Image Vis. Comput.*, vol. 28, no. 4, pp. 668–676, 2010.
- [24] M. F. Talu, "ORACM: Online region-based active contour model," *Expert Syst. Appl.*, vol. 40, pp. 6233–6240, Nov. 2013.
- [25] K. Hanbay and M. F. Talu, "A novel active contour model for medical images via the Hessian matrix and eigenvalues," *Comput. Math. Appl.*, vol. 75, pp. 3081–3104, May 2018.
- [26] B. Han and Y. Wu, "Active contours driven by global and local weighted signed pressure force for image segmentation," *Pattern Recognit.*, vol. 88, pp. 715–728, Apr. 2019.
- [27] H. Zhang, J. E. Fritts, and S. A. Goldman, "An entropy-based objective evaluation method for image segmentation," *Proc. SPIE*, vol. 18, pp. 38–49, Dec. 2003.
- [28] J. Fang, H. Liu, L. Zhang, J. Liu, and H. Liu, "Fuzzy region-based active contours driven by weighting global and local fitting energy," *IEEE Access*, to be published. doi: [10.1109/Access.2019](https://doi.org/10.1109/Access.2019).
- [29] L. Fang, T. Qiu, Y. Liu, and C. Chen, "Active contour model driven by global and local intensity information for ultrasound image segmentation," *Comput. Math. Appl.*, vol. 75, no. 12, pp. 4286–4299, Jun. 2018.
- [30] H. Wang, T.-Z. Huang, Z. Xu, and Y. Wang, "A two-stage image segmentation via global and local region active contours," *Neurocomputing*, vol. 205, no. 12, pp. 130–140, Sep. 2016.



JIANGXIONG FANG received the B.S. and M.S. degrees from Central South University, Changsha, China, in 2004 and 2007, respectively, and the Ph.D. degree in pattern recognition and intelligent systems from the Institute of Image Processing and Pattern Recognition, Shanghai JiaoTong University, Shanghai, China, in 2012. He is currently an Associate Professor (Teacher) with the East China University of Technology. His research interests include image segmentation and machine learning.



HUAXIANG LIU received the B.S. and M.S. degrees in circuits and systems from Hunan Normal University, in 2007 and 2010, respectively. She is currently a Teacher with the East China University of Technology. Her research interests include remote sensing image processing, convex optimization problem, variational theory for image segmentation, and visual object tracking and detection.



JUN LIU received the B.S. and M.S. degrees from the Shenyang University of Technology, Shenyang, China, in 2003 and 2006, respectively, and the Ph.D. degree in detection technology and automation devices from Northeastern University, Shenyang, China, in 2010. He is currently an Associate Professor (Teacher) with the East China University of Technology. His research interests include metallurgical parameters detection and image processing.



LITING ZHANG received the M.S. degree from the East China of Technology, Fuzhou, China, in 1990, the B.S. degree from the Hefei University of Technology, Hefei, in 1999, and the Ph.D. degree in cartography and geographic information engineering from Wuhan University, Wuhan, China, in 2006. His research interests include remote image processing, and GIS theory and application.



HESHENG LIU received the B.S., M.S., and Ph.D. degrees from Shanghai JiaoTong University, Shanghai, China, from 1981 to 1990. He was selected as the New Century National Hundred, Thousand and Ten Thousand Talent Project in China and Special allowance of the State Council. He is currently a Professor and is serving as the President of the East China University of Technology. His research interests include mechanical and electrical integration, advanced control systems, and optimization algorithm.

• • •